IIETA International Information and Engineering Technology Association
Advancing the World of Information and Engineering

Traitement du Signal
Vol. 40, No. 6, December, 2023, pp. 2383-2395
Journal homepage: http://iieta.org/journals/ts

A High-Performance, Equus Jubatus-Optimized Deep Learning Model for Satellite Image-Based Change Detection

Chafle Pratiksha Vasantrao, Neha Gupta*

School of Electronics Engineering, VIT-AP University, Amaravati 522237, India

Corresponding Author Email: neha27brs@vitap.ac.in

https://doi.org/10.18280/ts.400605

Received: 19 May 2023
Revised: 31 July 2023
Accepted: 8 September 2023
Available online: 30 December 2023

Keywords:
hybrid deep fusion model, segmentation, change detection, Equus Jubatus optimization, multispectral images

ABSTRACT

The ability to detect changes in Earth's surface using satellite imagery is a crucial tool for monitoring and managing the dynamic terrestrial transformations. This process, however, necessitates the continuous refinement of techniques within the field of remote sensing. In this study, an advanced hybrid deep fusion model, underpinned by the Equus Jubatus optimization algorithm, is presented for effective change detection in satellite imagery. This novel fusion model is the result of a hybridization of pre-trained models, encompassing Fully Connected DenseNet (FC-DenseNet), Res-U-Net, U-Net, and SegNet, which collectively optimize fusion parameters. The Equus Jubatus optimization algorithm, central to this process, promotes rapid convergence while reducing computational complexities. This proposed model generates binary change maps from bitemporal satellite images, with experiments conducted using optical satellite images sourced from the Landsat satellite. Performance was assessed across three different databases, yielding an accuracy of 0.963 and an F1 score of 0.904 for Database 1, an accuracy of 0.895 and an F1 score of 0.812 for Database 2, and an accuracy of 0.819 and an F1 score of 0.862 for Database 3. These results suggest that the proposed model offers superior performance in comparison to existing state-of-the-art techniques.

1. INTRODUCTION

A country's wealth is significantly tied to its natural assets, underscoring the importance of nature preservation. Remote sensing technology, particularly Change Detection, plays a pivotal role in this regard due to its ability to monitor the ecosystem's dynamic transformations. Natural disasters, by causing soil erosion, climatic changes, drought, and floods, necessitate the implementation of reliable and accurate change detection measures.

Change detection, via remote sensing, is employed to extract and predict changes in geographical regions through repeated observations. This technology is instrumental in examining land cover and land use changes, monitoring vegetation, forest changes, and environmental shifts, studying urbanization, managing resources, and controlling disasters like forest fires and floods [1-3]. The recent surge in predicting these changes has emerged as a key aspect of Earth observation, finding extensive applications in fields like environmental monitoring, disaster management, urban development, and military operations [4-10].

Current research trends focus on identifying surface water fluctuations as an indicator of anthropogenic, environmental, and climatic activities. Remote sensing images prove invaluable in tracking geographical and temporal fluctuations in water surfaces, including lakes, reservoirs, and rivers. Change prediction through multitemporal images has been under study for several decades. Classical change detection models in remote sensing are categorized into three groups: image arithmetic-based models, image transformation-based models, and object classification-based models [8, 11].

Before the advent of advanced Deep Learning (DL) models, the challenges in predicting changes were addressed by physically modeling a complex set of features, necessitating a significant level of expertise and precision [12]. Leveraging technology for predicting surface changes is both cost-effective and reduces manual labor. The features derived from remote sensing images depend on physical interpretation and the availability of high-resolution satellite data [13].

This section provides a comprehensive introduction to various existing models proposed by different researchers for change detection prediction, outlining their advantages and drawbacks. Recently, DL methods have demonstrated exceptional performance in image analysis. The Fully Convolutional Network (FCN) model, for instance, has been primarily used for change detection in remote sensing images [14]. Despite its effectiveness, FCN struggles to detect minute changes in satellite images.

Other efforts, such as the Dual Attentive Fully Convolutional Siamese networks (DASNet) by Chen et al. [2], Generative Adversarial Networks (GAN) by Lei et al. [15], and novel Cross Layer Convolutional Neural Network (CLNet) by Zheng et al. [12], have made significant contributions to the field. However, each of these models presents its own set of limitations, including heavyweight model parameters, increased computational time, and

difficulty in targeting specific points.

The following sections delve deeper into these research efforts, their workings, challenges, and contributions. Section 2 presents the challenges and contributions, Section 3 explains the working of the proposed Equus Jubatus optimization-based fusion network and its architectural models, and also outlines the mathematical model of the Equus Jubatus optimization and its function. The results obtained are discussed in Section 4, and the research concludes in Section 5.

2. CHALLENGES AND CONTRIBUTION

As we know, change detection depends on the analysis of bitemporal remote sensing images. Bitemporal images suffer from radiometric variations that is caused by atmospheric factors and lighting conditions. These variations alter the values of the pixels significantly, even though there is no change at any location. This process makes the change detection difficult. Hence, development of such technique which can easily detect the changes is important research topic in the remote sensing. As stated above, deep learning models are able to produce promising results, however, they lack in few important points. First, few models fail to detect minute changes. Second, few models use more parameters, which makes them heavyweight model. Third, few technique are unable to locate the targeted point. The proposed model will solve the aforementioned problem by fusion and optimization strategies. By combining several models, the new framework will make use of each model's advantages and extract additional characteristics from the input data. In recent studies, it has been noticed that fusion is incorporated to generate more reliable features and results in many research areas. Ren et al. [16] adapted cross-modal sensing text-image retrieval model that integrated different levels of features with multi-level information (local and global information) dynamic fusion module. The fusion module used in this research utilises local information for correcting global information, in addition to utilising global information to support the local information. Along with this, incorporating optimization into deep learning models will reduce computation complexities by reducing the model's parameters. Sheoran et al. [17] introduced the Ant Colony Algorithm, Particle Swarm Optimization and Genetic Algorithm provided superior quality change detection results by finding more edges. Motivated by aforesaid advantages, the research aims to devise an efficient DL-based change detection approach. The proposed deep learning model is the fusion of four deep learning models with Equus jabutas optimization. The following is an outline of the contributions that the research has done.

1) Initially, the input remote sensing image is taken from the database. Furthermore, in the preprocessing step, satellite images are resized to obtain a balanced image size. Then normalization is performed to obtain a similar distribution for faster convergence. After that, thematic information discrimination or important features in remote sensing images are derived from vegetation indices by making use of preprocessed satellite images. This reduces the computational complexity significantly.
2) Hybrid deep fusion model is developed for pixel variation analysis, which segments the image to locate the changes along with the boundaries. The segmentation includes labelling of pixels and then detecting the changes in the corners. The fusion model is proposed using the fully connected DenseNet [18], SegNet [19], Res U-Net [20], and U-Net [21, 22]. Every deep learning model has a different architecture and capacity for feature representation. By combining several models, the new framework may make use of each model's advantages and extract additional characteristics from the input data. As the proposed fusion model contains four deep learning model, these are the advantages of each model being used in the change analysis: 1) It minimizes the number of parameters and detect minute changes; 2) It provide high performance with a low number of parameters and prevent the loss of information; 3) It required low number of training samples for segmentation. It tracks down the minute lost information and permits fast convergence; 4) It reduce complexities in computation and availability of skip connections help to speed up the training process. Res U-net and U-Net models are helping to get the boundaries detection because it prevents the loss of information. Each model offers a unique set of predictions, and by integrating these predictions using fusion techniques like weighted averaging or decision-level fusion, the results of change detection can be more accurate overall and less likely to contain false positives or false negatives. As a result, change detection has increased discriminative capability and better representation of pixel-level differences. The fusion output for the proposed hybrid deep learning model is obtained by hybridizing the outputs from four pertained model.
3) This contribution includes the optimization strategy for determining the fusion parameters. Here, Equus Jubatus optimization-based fusion model is developed by hybridizing the outputs from four pertained model and the optimal solution is determined by tuning the parameters. The Equus Jubatus optimization is developed by the combining of the Horse Herd Optimization Algorithm (HHOA) [23] and Cheetah Chase Optimization Algorithm (CCOA) [24]. Ponies or Equus are energetic animals that exhibit six behavior patterns. It provides the strength between exploitation and exploration space. On the other hand, Jubatus is the fastest predator on earth. The high-speed chasing behavior of the Jubatus enhances the convergence speed of the optimization. The characteristics of the Equus-Jubatus algorithm build up with the searching behavior of ponies and the fast speed nature of the cheetah to reduce complexities in the computational process with faster convergence characteristics.

3. PROPOSED EQUUS-JUBATUS OPTIMIZATION-BASED HYBRID DEEP FUSION MODEL FOR THE CHANGE DETECTION

DL-based segmentation methods are widely employed for the detection method. Initially, the input remote sensing images are taken from the database. Furthermore, in the data preprocessing phase, the raw and unbalanced satellite images are resized and processed using the geometric correction technique. Now, the obtained balanced image size is subjected to normalization using the image normalization method to obtain a similar distribution of satellite images, which will help to get the faster convergence. After that, thematic

information discrimination or important features in satellite images is derived from vegetation indices by making use of preprocessed satellite images. This reduces the computational complexity significantly. The proposed pixel variation analysis is carried out to segment the input image. The segmentation includes labelling pixels for binary change detection. The pixelwise change detection output is achieved by using the hybridized pre-trained classifier, viz., fully connected dense net, Res-U-net, SegNet, and U-Net. The developed model is having the simplest training process along with fewer parameters. The final detection output is generated through the fusion factor that is optimally designed using the proposed Equus-Jubatus. Equus-Jubatus optimization generates the fusion parameters to facilitate scalar values for combining the multiple decision information, which provides better classification outcomes and reduces the complexities in the computational process with faster convergence characteristics. Figure 1 shows the overview of proposed model. Further, we present the steps of the proposed technique.

3.1 Read the input

The input satellite images are taken. Let the total images extracted from the databases be denoted as

$$a = F_b \tag{1}$$

where, a represents the dataset, F_b represents the images present in the databases, and b denotes the total number of images. From the whole data, sixty percent of the data are utilized as training samples, and forty percent of the data are used as testing samples.

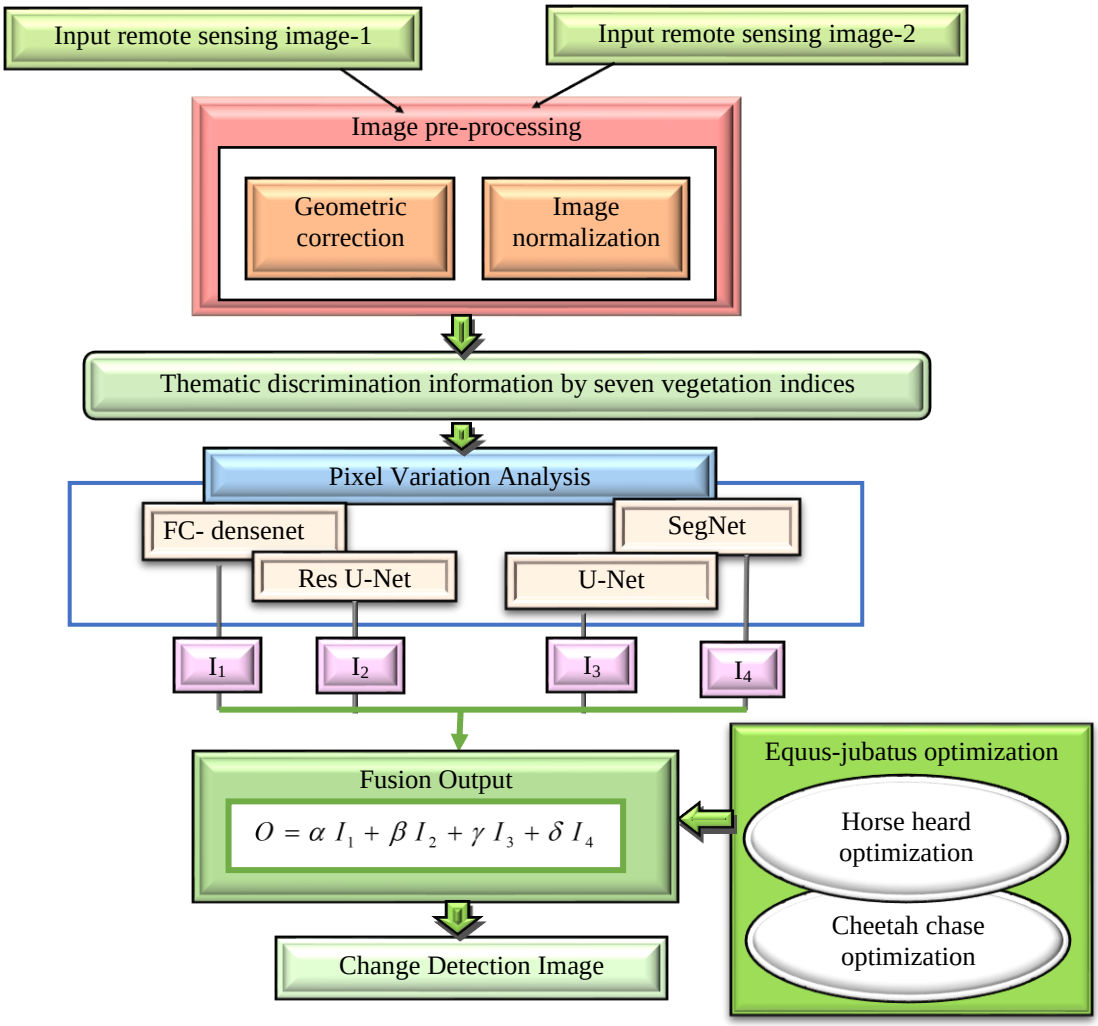

Figure 1. An overview of the proposed model

3.2 Image pre-processing

Once the raw satellite images are gathered from the databases, pre-processing is carried out, which processes the natural satellite images. The satellite databases consist of noise and other deprivation that might negatively influence the accuracy of the system. Preprocessing enhances the quality of the image by eliminating the distortions and noise of the image. In this research, preprocessing is performed using geometric correction [25] and image normalization [26] methods.

3.2.1 Geometric correction

Geometric correction is an important step in processing the satellite image, which eliminates the geometric distortions to align the individual pixel in orderly planimetric (c', d') locations on the map. The geometric correction enhances the spatial coincidence of the image and minimizes the geometric distortion error to ensure the proper position of features in the image. Geometric correction permits the processed image to be compared with the reference data for the generation of precise location, details regarding the direction and polygonal

area. For a set of surface sample points $\{b_c\}_{c=1}^{A}$ calibrating the parameters of the projector-camera network, this enables us to warp the projected image into the camera's frame to make it appear as although the camera is looking at the projected imagery. The geometry of the display surface and the calibration of the projector and camera serve as the sole determinants of this mapping to study the compensation function for the geometric distortion $B^{-1}(\cdot)$, and to evaluate the geometric features between the projector and camera pixels on the display surface.

$$\left\{b_{C'}\right\}_{c=1}^{A} = B^{-1}\left(\left\{b_{D'}\right\}_{c=1}^{A}\right) \tag{2}$$

Here, the compensation function for the geometric distortion $B^{-1}(\cdot)$ is piecewise linear and it plots all the surface sample points in the projector aspect $\{b_{D'}\}_{c=1}^{A}$, to the related points $\{b_{C'}\}_{c=1}^{A}$ in the camera aspect. The linear piecewise data conduct the triangulation method on all the surface sample points next to determine the best compensation value for the geometric distortion and predictor the image to be predicted; hence the obtained image is corrected geometrically.

3.2.2 Image normalization

The illumination condition and atmospheric effects may cause radiometric variations hence the applied image normalization step normalizes the image to an equal and common radiometric scale that will make a considerable impact in optimization [27]. Image normalization is essential in image processing because it minimizes the radiometric effects of nonsurface factors, which makes computation efficient. Image normalization changes the intensity values of the pixels and brings the distorted image into a normal viewable range. The affine transformation matrix helps to generate a normalized image and let $\lambda_{e'f'}$represent the central moment of a digitally obtained image $h(c', d')$ of size $E \times F$ where,

$$\lambda_{e'f'} = \sum_{c'=0}^{E-1}\sum_{d'=0}^{F-1}\left(c' - \overline{c'}\right)^{e'}\left(d' - \overline{d'}\right)^{f'} h\left(c', d'\right) \tag{3}$$

$$\overline{c'} = \frac{\sum_{c'=0}^{E-1}\sum_{d'=0}^{F-1} c' h\left(c', d'\right)}{\sum_{c'=0}^{E-1}\sum_{d'=0}^{F-1} h\left(c', d'\right)} \tag{4}$$

$$\overline{d'} = \frac{\sum_{c'=0}^{E-1}\sum_{d'=0}^{F-1} d' h\left(c', d'\right)}{\sum_{c'=0}^{E-1}\sum_{d'=0}^{F-1} h\left(c', d'\right)} \tag{5}$$

XYS-based image normalization: The homogeneous affine transformation matrix is decomposed into $\overline{c'}$ shearing, $\overline{d'}$ shearing and scaling anisotropic matrices,

$$B' = \begin{bmatrix} g'_{11} & g'_{12} \\ g'_{21} & g'_{22} \end{bmatrix} = \begin{bmatrix} \chi & 0 \\ 0 & \mu \end{bmatrix}\begin{bmatrix} 1 & 0 \\ \eta & 1 \end{bmatrix}\begin{bmatrix} 1 & \varepsilon \\ 0 & 1 \end{bmatrix} \tag{6}$$

$\chi, \varepsilon, \eta, \mu \in A'$ which uses constraints in some cases $\lambda_{31} = 0, \lambda_{13} = 0, \lambda_{20} = 1, \lambda_{02} = 1$, where A' denotes the scalar factor of the affine matrix.

3.3 Thematic information discrimination

From pre-processed remote sensing images, thematic information discrimination in satellite images are derived from vegetative indices [21] such as the normalized difference vegetation index (NDVI) [28, 29], global environmental monitoring index (GEMI) [30], modified soil-adjusted vegetation index (MSAVI) [28], relative vigor index (RVI), modified simple ratio (MSR) [31], weighted difference vegetative index (WDVI) [32], and soil adjusted vegetative index (SAVI) [28, 30]. WDVI is a nonlinear index utilized to track global vegetation from remote sensing images. The NDVI is the widely utilized vegetative index that signifies the striking contract between red spectral reflectance and NIR. The SAVI is utilized for the correction of NDVI from the impacts of soil brightness in low vegetative regions. The MSAVI is the extended version of SAVI with an inductive function that is used to minimize the soil effects. The MSR is the ratio of the near-infrared to red brightness value, and the RVI is utilized to determine the stress level of the crop. The WDVI is defined as the ratio between the NIR and red reflectance, and it is used to overcome the perpendicular vegetative index due to brighter soil. To reduce computational complexity, the proposed method uses aforementioned seven vegetation indices to thematically discriminate preprocessed satellite images.

3.4 Pixel variation analysis using the proposed hybrid deep fusion model

In the pixel variation analysis, the processed satellite image is analysed pixelwise to detect the changes in the satellite image [33]. The pixel variation is crucial in change detection of small-scale changes where the conventional methods lag. Therefore, a method, which captures subtle differences in the pixel values, is used in this research and is computationally efficient that overcomes the complex algorithms. In this paper, the pixel variation analysis analysis is established using hybrid deep fusion model, which comprises fully convolutional networks, such as fully connected DenseNet, SegNet, Res U-Net, and U-net. The fusion parameters in the proposed hybrid deep fusion model are acquired using the proposed Equus-Jubatus optimization. Figure 2 shows the architecture of the proposed hybrid deep fusion model. The utilized pre-trained models are described in the following section.

3.4.1 FC-DenseNet

FC- DenseNet is utilized for pixel variation analysis because it mitigates the vanishing gradient issue, enhances feature reuse, supports the feature propagation and minimizes the number of parameters. The densely connected convolutional network is extended for classifying the images upon including an upsampling medium to generate an FC-DenseNet for pixelwise analysis of the satellite image. FC-DenseNet has the capability to reuse the information from the previous layer, and integrates the computed feature maps at every layer along with the generated features of the preceding layer forming a dense block. Every block comprises ReLU activation, batch normalization, dropout, and a 3×3 convolution layer. FC-DenseNet employs transition-up modules and dense blocks in the upsampling medium that upsamples the feature maps by converting the convolution to the original resolution of an image. To recover minute information, complex connections were also implemented in FC-DenseNet.

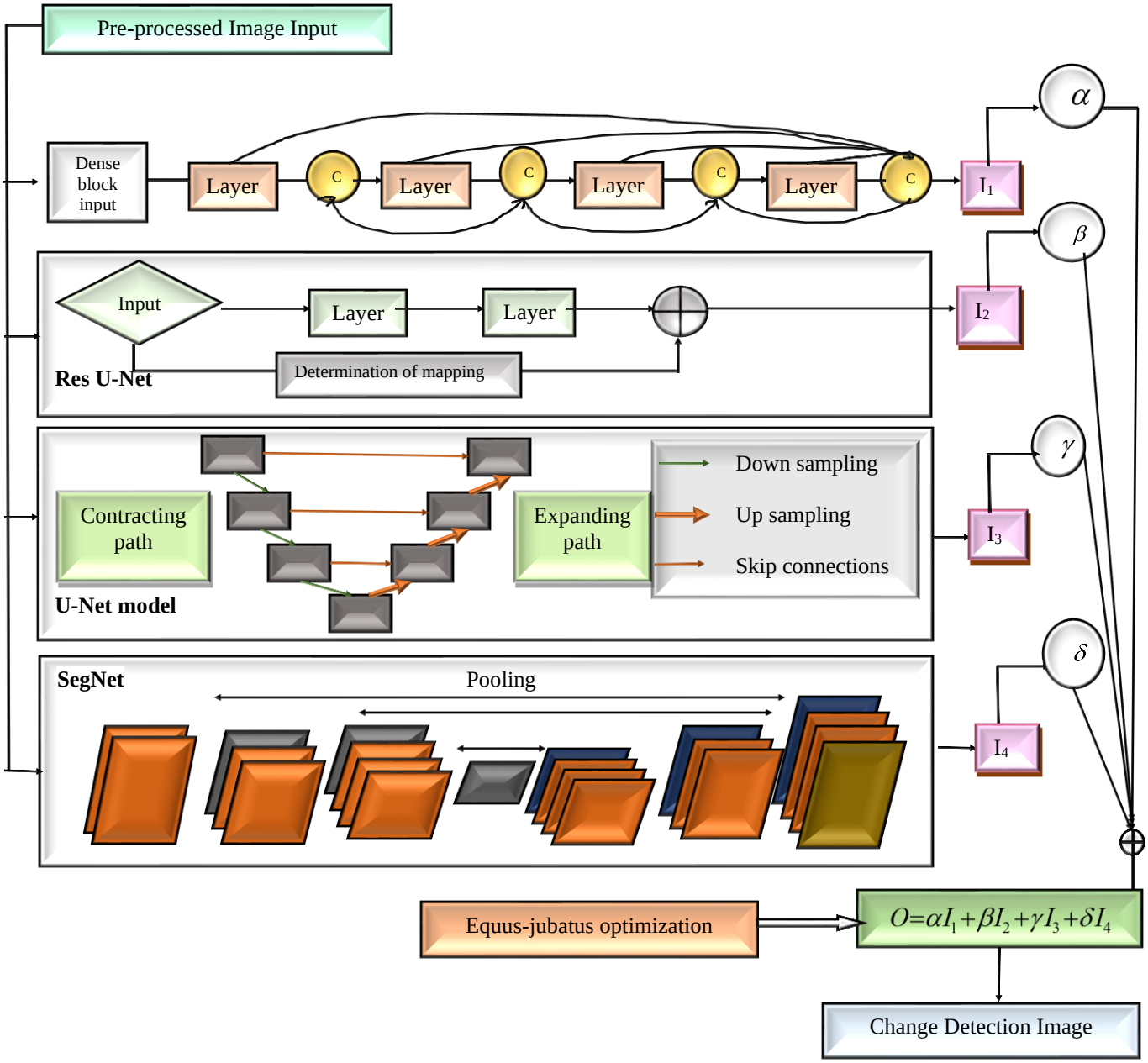

Figure 2. Architecture of the proposed Equus Jubatus optimization enabled hybrid deep fusion model

3.4.2 Res U-Net

Res U-Net is a fully convolutional neural network that combines residual block and the U-Net model for classifying the processed satellite image. The Res U-Net will provide high performance with a low number of parameters. The residual unit does not allow the accelerating or fading gradient issue and assists in developing deep networks. In addition, rather than mapping the input-to-output, the residual unit will study the residual for adding to the input to generate the output. The Res U-Net comprises stacked residual units in the encoder-decoder system in encoding stage, a 1×1 convolution along with two advanced down samples of the residual unit output at every stage. In the decoder stage, the layers in the upsampling expand the spatial resolution until it reaches the images original size. The complex connections were included in this model to prevent the loss of information at the encoder stage.

3.4.3 U-Net

U-Net provides better segmentation performance for the segmentation process with a low number of training samples**.** The U-Net is primarily used for classifying images and comprises two sequential phases. An encoder efficiently decreases the spatial resolution due to increased extraction of unrefined features. Next, a decoder network continues to extract characters with higher resolution in increasing order until it attains actual resolution and connects a group to every position of the input pixel. The main characteristic feature of the U-Net model is skipped connections, which connect the captured features in the downsampling medium to the computed characters through the related layers of the upsampling medium. Hence, this technique tracks down the minute lost information using the pooling functions and permits fast convergence.

3.4.4 SegNet

SegNet is widely accepted technique for image labelling, as it provides smooth label predictions, improves the accuracy and visualizes feature activation effects**.** One of the major characteristics of the SegNet is decoding, where the max-pooling behavior in the encoder phase decreases the spatial

resolution and complexities in computation, resulting in the loss of spatial details and negative effects in the output, mainly at the borders of the object. SegNet tries to control this by depositing the indices of maximal pooling in the encoder and employing them to track down the important details of the location of the upsampling performance at the relevant decoder phase. The skip connections help to speed up the training process because there is no need to learn weights in the upsampling phase.

Further, to obtain fusion output, a hybrid deep fusion model is developed by combining fully convolutional networks, viz., FC-DenseNet, Res U-Net, U-Net and SegNet. The integration is carried out by using the fusion parameters α, β, γ, and δ. These fusion parameters are determined by using the proposed Equus-Jubatus optimization algorithm.

Let us assume that the output from FC-DenseNet, Res U-Net, U-Net and SegNet is denoted as, I_1, I_2, I_3, and I_4, which are fused using the optimal fusion parameters to generate the final segmentation output that displays the changes in satellite images. Let the final segmented output generated using the proposed hybrid deep fusion model be given as O.

$$O = \alpha I_1 + \beta I_2 + \gamma I_3 + \delta I_4 \tag{7}$$

where, α, β, γ, and δ are the fusion parameters determined using the proposed Equus-Jubatus optimization.

The proposed model is able to detect the minute changes and boundaries information because of availability of Res U-Net and U-net. In addition, it provides high performance with a low number of parameters. Along with that the availability of the skip connections help to speed up the training process. and reduce complexities in computation.

3.5 Proposed Equus-Jubatus optimization algorithm

The proposed Equus-Jubatus algorithm is developed by combining the herding behavior of ponies [23] otherwise known as Equus and the fast prey hunting strategy of Jubatus [24] otherwise known as cheetah. The ponies have some important characteristics such as herding behavior and leadership behavior. They obey the leaders and can adapt themselves to any kind of environment quickly. They are explorers in nature, this behavior helps to attain global solutions meanwhile it follows the fight-or-flight strategy for defense. However, they lag in speed, hence, the speed updating phase in proposed optimization is integrated using the speed behavior of cheetah to attain the global best solution in less time. The Equus-Jubatus algorithm is used for the segmentation of the labeling pixel and the finest tuning of the fusion parameter in the pre-trained classifier. The consequence outcomes attained from the hybridized pre-trained models are optimally tuned from the fusion parameter using the Equus-Jubatus algorithm method for detecting changes in satellite images. The traditional optimization algorithms [34] reveal the features attained based on hunting behaviors that concentrate to attain a faster convergence rate but fail to provide the global optimal solution. Hence, a new algorithm known as Equus-Jubatus is proposed in this research article to provide a global optimal solution by avoiding premature convergence. A elaborate explanation of the proposed Equus-Jubatus algorithm is provided in this section.

3.5.1 Motivation

The proposed Equus-Jubatus algorithm imitates the behavior of ponies and Jubatus. Ponies are energetic animals that exhibit six behavior patterns, foraging, grazing, sociability, hierarchy, imitation, and defense, which generally vary depending on their age. This feature helps to attain the global best solution, as it provides the strength between exploitation and exploration space. On the other hand, Jubatus is the fastest predator on earth and utilizes its maximum speed to obtain prey. The high-speed chasing behavior of the Jubatus enhances the convergence speed of the optimization. Hence, integrating these two characteristics is the global best solution along with maximum convergence rate. The characteristics of the Equus-Jubatus algorithm build up with the searching behavior of ponies and the fast speed nature of the cheetah to attain the best solutions are mathematically expressed below.

3.5.2 Mathematical model for the proposed Equus-Jubatus algorithm

In this section, the performance of the ponies is mathematically summarized on its various characteristics as follows:

(1) Initialization stage: In the initialization stage, the location of the ponies is initialized based on the current location. The motion of the horses for iteration counts is given as follows,

$$G_d^{t,O'} = H_d^{t,O'} + G_d^{(t-1),O'}, O' = \mu, \varepsilon, \omega, \eta \tag{8}$$

where, $G_d^{t,O'}$ represents the location of the pony, O' indicates the range of age groups of the observed ponies, t represents the present iteration, and $H_d^{t,O'}$ represents the velocity of the pony. The variable η represents the ponies at age groups 0 to 5 years, ω represents the ponies at age groups 5 to 10 years, ε represents the ponies at age groups 10 to 15 years and μ represents the ponies above 15 years. The ponies are arranged on the basis of the best solutions 10% of ponies with higher ranks are picked as μ, the next 20% ponies are in ε, 30% ponies in ω and the remaining 40% ponies are in η. The speed of ponies at various age groups is mathematically given as:

$$H_d^{t,\mu} = J_d^{t,\mu} + K_d^{t,\mu} \tag{9}$$

$$H_d^{t,\varepsilon} = J_d^{t,\varepsilon} + L_d^{t,\varepsilon} + M_d^{t,\varepsilon} + K_d^{t,\varepsilon} \tag{10}$$

$$H_d^{t,\omega} = J_d^{t,\omega} + L_d^{t,\omega} + M_d^{t,\omega} + N_d^{t,\omega} + K_d^{t,\omega} + Q_d^{t,\omega} \tag{11}$$

$$H_d^{t,\eta} = J_d^{t,\eta} + N_d^{t,\eta} + Q_d^{t,\eta} \tag{12}$$

where, $J_d^{t,\mu}$ represents the parametric motion for the age of $\mu > 15$ in d^{th} ponies, $L_d^{t,\varepsilon}$ represents the velocity for the best ponies location, where $O' \leq 10 \geq d \; to \; \varepsilon \leq d \geq 15$, $K_d^{t,\mu}$ represents the escaping vector motion for the age as $\mu > 15$ in d^{th} ponies, $M_d^{t,\varepsilon}$ represents the vector of sociability motion metrics, where $O' \leq 10 \geq d \; to \; \mu \leq d \geq 15$, $N_d^{t,\omega}$ represents the orientation vector motion of the age from $O' \leq 5 \geq d \; to \; \omega \leq d \geq 10$, $Q_d^{t,\eta}$ represents the arbitrary velocity of the vector in d^{th} ponies where $O' \leq 0 \geq d \; to \; \eta \leq d \geq 5$.

(2) Herding strategy: Ponies are pasteurizing animals that feed on grasses, forages and plants and they herd on the grass land for approximately 16 to 20 hours a day with less

time for relaxation. The herding process of ponies is described as continual eating the region of grazing around each pony is represented as a precise location and the herding strategy is mathematically represented as:

$$J_d^{t,O'} = e_t\left(h' + \theta k'\right)\left[G_d^{(t-1)}\right], \quad O' = \mu, \varepsilon, \omega, \eta \tag{13}$$

$$e_d^{t,O'} = e_d^{(t-1),O'} \times \psi_e \tag{14}$$

where, $J_d^{t,O'}$ represents the motion of the j^{th} pony, which represents the aptness of the pony to herd and decreases the linearity value with ψ_e for each iteration, h' and k' represents the lower and upper limits of the grazing region whose values are 0.95 and 1.05, respectively. θ denotes a random number ranging from 0 to 1, and e is the coefficient, which is equal to 1.5 for all age classes.

(3) Leadership strategy: The ponies follow the instructions and guidance developed by the leader and the leaders are mostly human beings. In some cases, the elder ponies take care of the team and here is the coefficient that represents the team of horses to obey the elder pony of the group, which is mathematically formulated as:

$$L_d^{t,O'} = f_d^{t,O'}\left[G_*^{(t-1)} - G_d^{(t-1)}\right], \quad O' = \mu, \varepsilon \text{ and } \omega \tag{15}$$

$$f_d^{t,O'} = f_d^{(t-1),O'} \times \psi_f \tag{16}$$

where, $L_d^{t,O'}$ represents the effects of the best optimal location of pony on the speed parameter and $G_*^{(t-1)}$ represents the location of the best pony.

(4) Adaptable strategy: Ponies possess adaptable characteristics, as they are adaptable to the environment and mingle with other animals. The herding nature of the pony is considered a safety measure since it protects the ponies from hunting animals. Multiculturalism preserves the life expectancy of the ponies and because of their similar traits some ponies fight with each other, while some are enthusiastic about sheep and cattle. This nature of pony is considered the motion towards the average location of other ponies and is denoted as, *l*. It can be clearly identified that the ponies from age groups 5 to 15 years are interested in joining in the herd and are mathematically represented as:

$$M_d^{t,O'} = l_d^{t,O'}\left[\left(\frac{1}{R}\sum_{i=1}^{R} G_i^{(t-1)}\right) - G_d^{(t-1)}\right], \quad O' = \varepsilon, \omega \tag{17}$$

$$M_d^{t,O'} = l_d^{(t-1),O'} \times \psi_l \tag{18}$$

where, $M_d^{t,O'}$ represents the organized movement of j^{th} pony, $l_d^{t,O'}$ represents the respective orientation of pony towards the team in t^{th} iteration count, $l_d^{t,O'}$ reduces by a value of ψ_l in every iteration count, and R represents the total ponies.

(5) Mocking strategy*:* Ponies copy the characteristic traits of each pony and study their characters. This copying nature of the pony is represented as:

$$N_d^{t,O'} = k_d^{t,O'}\left[\left(\frac{1}{R_{best}}\sum_{i=1}^{R_{best}} \hat{G}_i^{(t-1)}\right) - G^{(t-1)}\right], \quad O' = \omega \tag{19}$$

$$k_d^{t,O'} = k_d^{t-1,O'} \times \psi_k \tag{20}$$

where, $N_d^{t,O'}$ represents the movement of j^{th} the pony towards the average of the best pony with the best $\hat{G}$ location, R_{best} represents the number of ponies with the best optimal location and ψ_k denotes the reduction parameter.

(6) Defense strategy: Ponies use fight-or-flight mechanisms as a defense strategy, in order to protect themselves from hunters. The ponies contest for water and food and move away from the unsafe surroundings. The defense behavior of the pony is represented as; *g*. The defense strategy is denoted in the negative term and is mathematically formulated as:

$$K_d^{t,O'} = -g_d^{t,O'}\left[\left(\frac{1}{R_{worst}}\sum_{i=1}^{R_{worst}} \check{G}_i^{(t-1)}\right) - G^{(t-1)}\right], \quad O' = \mu, \varepsilon, \omega \tag{21}$$

The mathematical relation for keeping the pony away is given as follows:

$$g_d^{t,O'} = g_d^{(t-1),O'} \times \psi_g \tag{22}$$

where, $K_d^{t,O'}$ represents the disappearance parameter of j^{th} ponies from the worst locations $\check{G}$, R_{worst} represents the number of ponies with the worst optimal location and ψ_g denotes the reduction parameter.

(7) Meandering strategy: The ponies wander in nearby areas and graze for food and they are curious animals in search of new grasslands. The meandering behavior is represented by parameter *m* and the process is formulated as follows:

$$Q_d^{t,O'} = m_d^{t,O'}\theta G^{(t-1)}, \quad O' = \omega, \eta \tag{23}$$

$$m_d^{t,O'} = m_d^{(t-1),O'} \times \psi_m \tag{24}$$

where, $Q_d^{t,O'}$ the wandering speed parameter of the pony for the local optimal search location ψ_m represents the reduction factor. The speed of ponies of age class 0 to5 years is given as follows:

$$\begin{gathered} H_d^{t,\eta} = \left[e_d^{(t-1),\eta}\psi_e(h' + \theta k')\left[G_d^{(t-1)}\right]\right] + \\ \left[k_d^{t-1,\eta}\psi_k\left[\left(\frac{1}{R_{best}}\sum_{i=1}^{R_{best}} \hat{G}_i^{(t-1)}\right) - G^{(t-1)}\right]\right] + \\ \left[m_d^{(t-1),\eta}\psi_m\theta G^{(t-1)}\right] \end{gathered} \tag{25}$$

The speed of ponies of age class 5 to10 years is given as follows:

$$\begin{gathered} H_d^{t,\omega} = \left[e_d^{(t-1),\omega}\psi_e(h' + \theta k')\left[G_d^{(t-1)}\right]\right] + \\ \left[f_d^{(t-1),\omega}\psi_f\left[G_*^{(t-1)} - G_d^{(t-1)}\right]\right] + \\ \left[l_d^{(t-1),\omega}\psi_l\left[\left(\frac{1}{R}\sum_{i=1}^{R} G_i^{(t-1)}\right) - G_d^{(t-1)}\right]\right] + \\ \left[k_d^{t-1,\omega}\psi_k\left[\left(\frac{1}{R_{best}}\sum_{i=1}^{R_{best}} \hat{G}_i^{(t-1)}\right) - G^{(t-1)}\right]\right] - \\ \left[g_d^{(t-1),\omega}\psi_g\left[\left(\frac{1}{R_{worst}}\sum_{i=1}^{R_{worst}} \check{G}_i^{(t-1)}\right) - G^{(t-1)}\right]\right] + \end{gathered} \tag{26}$$

$$\left[m_d^{(t-1),\omega}\psi_m\theta G^{(t-1)}\right]$$

The speed of ponies of age class 10 to15 years is given as follows:

$$\begin{gathered} H_d^{t,\varepsilon} = e_d^{(t-1),\varepsilon}\psi_e(h'+\theta k')\left[G_d^{(t-1)}\right] + \\ f_d^{(t-1),\varepsilon}\psi_f\left[G_*^{(t-1)} - G_d^{(t-1)}\right] \\ +l_d^{(t-1),\varepsilon}\psi_l\left[\left(\frac{1}{R}\sum_{i=1}^{R} G_i^{(t-1)}\right) - G_d^{(t-1)}\right] - \\ g_d^{(t-1),\varepsilon}\psi_g\left[\left(\frac{1}{R_{worst}}\sum_{i=1}^{R_{worst}} \breve{G}_i^{(t-1)}\right) - G^{(t-1)}\right] \end{gathered} \tag{27}$$

The speed of ponies of age above15 years is given as follows:

$$\begin{gathered} H_d^{t,\mu} = e_d^{(t-1),\mu}\psi_e\left(h'+\theta k'\right)\left[G_d^{(t-1)}\right] - \\ g_d^{(t-1),\mu}\psi_g\left[\left(\frac{1}{R_{worst}}\sum_{i=1}^{R_{worst}} \breve{G}_i^{(t-1)}\right) - G^{(t-1)}\right] \end{gathered} \tag{28}$$

(8) Speed updating phase: The various characteristics of various age groups of ponies demonstrated that the lesser factor of velocity that can enhance the motion vector by inducing the character of Jubatus is to boost the speed of the classification and the variations in their age limit can be used according to the necessity, which consumes the less energy and reduces the time complexity. The velocity factor of the Jubatus is given by:

Table 1. Algorithm for the proposed Equus-Jubatus optimization-based fusion network

Sr.No.	Pseudo Code for the Proposed Equus Jubatus Optimization-Based Fusion Network
1.	Initialization stage
2	Herding strategy
3	Leadership strategy
4	Adaptable strategy
5	Mocking strategy
6	Defense strategy
7	Meandering strategy
8	Speed updating phase
9	Initialization stage
10	Initialize: $O' = \mu, \varepsilon, \omega, \eta$; $H_d^{t,O'}$
11	Configure
12	$G_d^{t,O'} = H_d^{t,O'} + G_d^{(t-1),O'}, O' = \mu, \varepsilon, \omega, \eta$
13	Herding strategy
14	if($i \leq 20$)
15	Pasteurize
16	Else
17	Rest
18	for ($O' = \mu, \varepsilon, \omega, \eta$)
19	Determine velocity factor: $J_d^{t,O'}$
20	end for
21	Leadership strategy
22	for ($O' = \mu, \varepsilon \, and \, \omega$)
23	Determine velocity factor: $L_d^{t,O'}$
24	end for
25	Adaptable strategy
26	for ($O' = \varepsilon, \omega$)
27	Determine the velocity factor: $M_d^{t,O'}$
28	end for
29	Mocking strategy
30	for ($O' = \omega$)
31	Determine the velocity factor: $N_d^{t,O'}$
32	end for
33	Defense strategy
34	for ($O' = \mu, \varepsilon, \omega$)
35	Determine the speed factor: $K_d^{t,O'}$
36	end for
37	Meandering strategy
38	for ($O' = \omega, \eta$)
39	Determine the speed factor: $Q_d^{t,O'}$
40	end for
41	Speed updating phase
42	$H_{best} = \{H_d^{t,\eta}, H_d^{t,\omega}, H_d^{t,\varepsilon}, H_d^{t,\mu}\} H_{j,p}$

$$H_{j,p} = H_{j,p} + q \times r \times \left(z_{best,p} - z_{j,p}\right) \quad (29)$$

where, p represents the position, j denotes the Jubatus and $H_{j,p}$ gives the velocity factor of the Jubatus. $z_{best,p}$ is the position of the best Jubatus with the best fitness value and $z_{j,p}$ is the position of the other Jubatus. The factor r represents the stable factor and the factor q denotes a random number in the range of [0,1].

Therefore, Eq. (29) shows that the proposed Equus-Jubatus-based optimization that enhances the segmentation based pre-trained method is effectively tuning the fusion parameter using the proposed method for more precise change detection in the multispectral images. The speed factor of ponies and Jubatus for achieving the best global solution is emphasized using the fine tuning of the proposed Equus-Jubatus-based optimization algorithm, which is expressed in Eq. (30).

$$H_{best} = \left\{H_d^{t,\eta}, H_d^{t,\omega}, H_d^{t,\varepsilon}, H_d^{t,\mu}\right\} H_{j,p} \quad (30)$$

In the above equation, the speed factors are boosted by integrating the speed of Jubatus $H_{j,p}$ with the velocity of the ponies at various ages $\{H_d^{t,\eta}, H_d^{t,\omega}, H_d^{t,\varepsilon}, H_d^{t,\mu}\}$. The algorithmic procedures of the proposed Equus-Jubatus based optimization are enumerated in Table 1.

As the proposed Equus-Jubatus algorithm imitates herding behavior of Equus or ponies and hunting behavior of Jubatus which has the characteristics, build up with the searching behavior of ponies and the fast speed nature of the cheetah. Therefore, integrating two things reduces complexities in the computational process using less number of parameters, provides global best solution and faster convergence. Whereas the traditional optimization algorithm may fail to get global best solution and faster convergence rate.

4. EXPERIMENTAL RESULTS

This section evaluates the results that are achieved of the proposed approach, and this subsection describes the results achieved.

4.1 Databases description

All three database images are described as follows.

(1) Database -1: The database is obtained from the Yambulla state forest in Australia by Landsat 8 (OLI). The size is approximately 320×260, captured on 01 October 2015 and 06 February 2016. The database encompasses the bushfire that occurred on the gold mine road in December [21, 26, 35-37].

(2) Database -2: The database is obtained from Natural Lake located in Rajasthan city, India, by Landsat 7 ETM+. The size is approximately 220×550, captured on 09 February 2001 and 21 September 2001. It demonstrates how the lack dried between these two dates [21, 26, 35-37].

(3) Database -3: The database is obtained from Bhopal using the Landsat 5 TM sensor. The size is approximately 206×424, captured on 29 May 2009 and 09 November 2011. The database encompasses the upper lake in the Bhopal region. This shows that the lakes dry between the two dates due to low rainfall [26, 35-37].

4.2 Performance metrics

The metrics used in evaluating the efficacy of the Equus-Jubatus optimization-hybrid deep fusion model is accuracy, precision, recall, and f1 measure [8, 13, 38].

4.3 Effect on number of epochs for fine tuning

The number of epochs is an important attribute, as it affects the tuning of the entire model and the performance of the classifier.

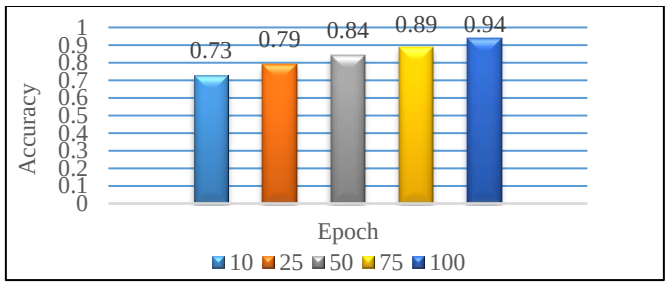

Figure 3. Illustrates the effect of number of epochs on the accuracy of the proposed model

Figure 3 Illustrates the number of epoch values increases when the sixty percent of the data are utilized as training samples, and forty percent of the data are used as testing samples in the proposed method. According to Figure 3, it can be observed that best performance can be achieved by 100 epochs.

4.4 Comparison methods and results

The change detection result is compared to the ground truth image during qualitative evaluation. In light of this, a visual comparison is made between the change detection result created by the proposed approach and the ground truth image. In the resulting binary map, black pixels represent the affected region and white pixels represent the unaffected region. Some previous approaches are used to compare the visual findings, such as Local Binary Similarity Pattern (LBSP) (MD1) [26], Deep Neural Network (DNN) (MD2) [39], U-NET (MD3) [40], SHO-build on UNET (Spotted hyena optimization) (MD4) [41], flamingo build on UNET (MD5) [42], Horse Herd Optimization Algorithm (HHOA) build on UNET (MD6) [23], and Cheetah Chase Optimization Algorithm (CCOA) build on fusion network (MD7) [24].

The databases, such as Yambulla state forest database, Natural lake database and Bopal city database input images are shown in Figure 4. (a)-(f), Figure 5. (a)-(f), Figure 6. (a)-(f). The ground truth in Figure 4. (g), Figure 5. (g), Figure 6. (g) indicate changes and no change information.

4.4.1 Comparative analysis

This research is presented with a novel Equus Jubatus optimization-dependent hybrid deep fusion model to detect the changes in the remote satellite images. Various conventional models were also present in the same field yet it holds some cons the proposed method is used to overcome these cons. The efficiency of the novel method is analyzed using the performance metrics such as accuracy, precision, recall, and f1 measures.

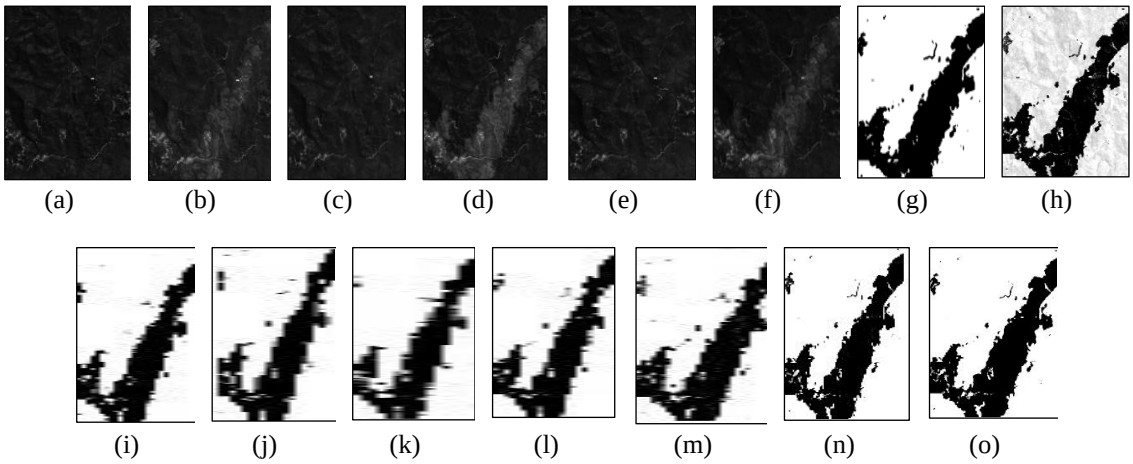

Figure 4. Various methods for identifying change detection in satellite images of the Yambulla State Forest database-1. (a) and (b) Landsat 8 OLI sensor RED channel satellite images from October 2015 and February 2016. (c) and (d) Landsat 7 ETM+sensor NIR channel satellite images from October 2015 and February 2016. (e) and (f) Landsat 5 TM sensor from GREEN channel satellite images from October 2015 and February 2016. (g) Ground truth image. (h), (i), (j), (k), (l), (m), (n) and (o) are change detection qualitative results for MD1, MD2, MD3, MD4, MD5, MD6, and MD7 and the proposed approach (MD8), respectively

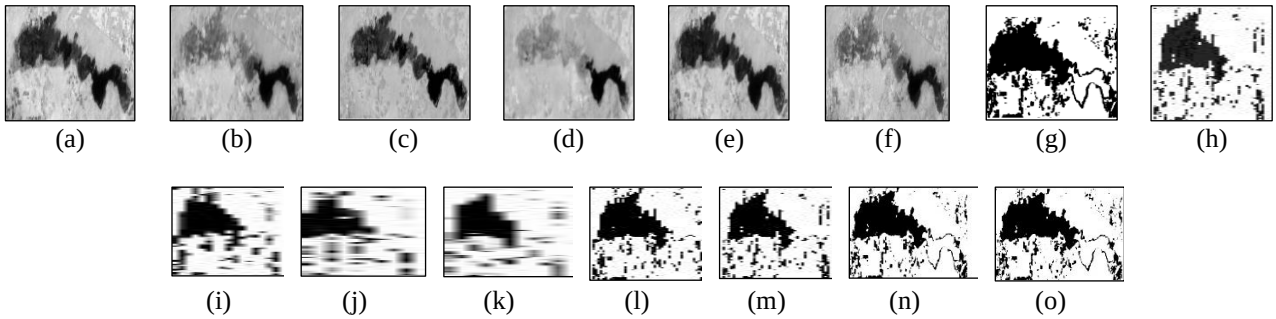

Figure 5. Various methods for identifying change detection in satellite images of Natural Lake database-2. (a) and (b) Landsat 8 OLI sensor RED channel satellite images. from February 2001 and September 2001. (c) and (d) Landsat 7 ETM+ sensor NIR channel satellite images from February 2001 and September 2001. (e) and (f) Landsat 5 TM sensor from GREEN channel satellite images from February 2001 and September 2001. (g) Ground truth image. (h), (i), (j), (k), (l), (m), (n) and (o) are change detection qualitative results for MD1, MD2, MD3, MD4, MD5, MD6, and MD7 and the proposed approach (MD8), respectively

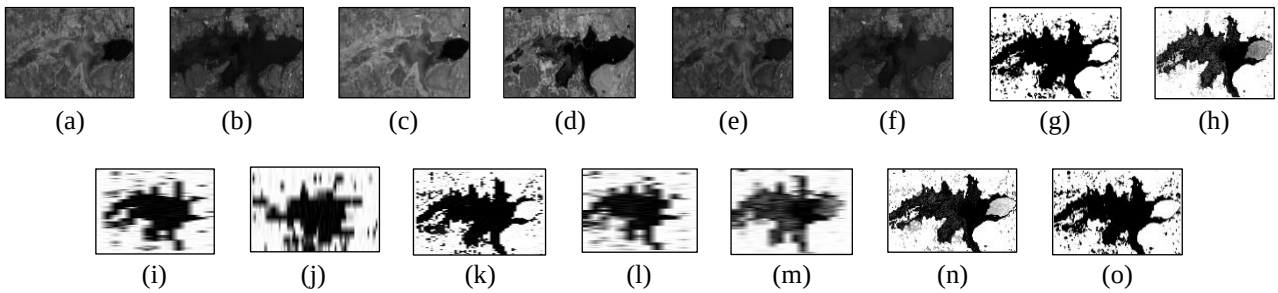

Figure 6. Various methods for identifying change detection in satellite images of Bhopal city database-3. (a) and (b) Landsat 8 OLI sensor RED channel satellite images from May 2009 and November 2011. (c) and (d) Landsat 7 ETM+ sensor NIR channel satellite images from May 2009 and November 2011. (e) and (f) Landsat 5 TM sensor from GREEN channel satellite images from May 2009 and November 2011. (g) Ground truth image. (h), (i), (j), (k), (l), (m), (n) and (o) are change detection visual results MD1, MD2, MD3, MD4, MD5, MD6, and MD7 and the proposed approach (MD8), respectively

This method has a high convergence rate and less computation time because of using optimization which is given in Figure 7.

4.4.2 Qualitative and quantitative results

The satellite image change detection visual results for MD1, MD2, MD3, MD4, MD5, MD6, MD7, and MD8 are shown in Figures 4(h)–(o), 5(h)–(o) and 6(h)–(o) for database-1, database-2 and database-3, respectively. Table 1 enumerates the achievements of proposed Equus Jubatus optimization enabled hybrid deep fusion model in terms of accuracy, precision, recall and f1 measure using database-1, database-2 and database-3.

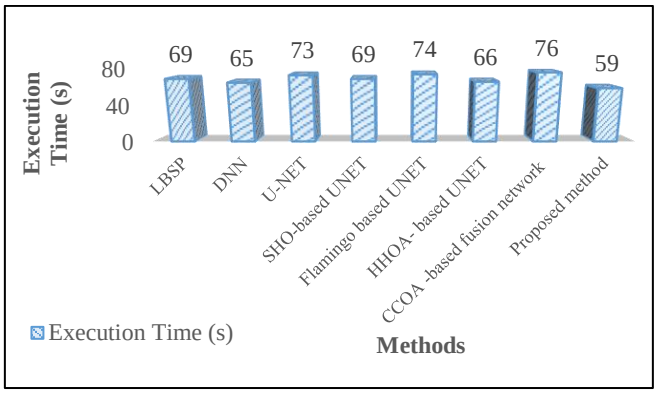

Figure 7. Comparison of execution time of proposed method with other conventional methods

4.5 Discussion

The proposed method getting better visual results because it is detecting minute and boundaries information as compare to other comparative analysis. The accuracy achieved by the developed approach based on database-1 is 0.963, while the previous approaches such as MD1, MD2, MD3, MD4, MD5, MD6, and MD7 obtained accuracies of 0.831, 0.917, 0.921, 0.922, 0.926,0.937 and 0.945 respectively. The accuracy achieved by the developed approach based on database-2 is 0.8951, while the previous approaches such as MD1, MD2, MD3, MD4, MD5, MD6, and MD7 obtained accuracies of 0.8571, 0.8647, 0.8670, 0.8789, 0.8825, 0.8867 and 0.8907 respectively. The accuracy achieved by the developed approach based on database-3 is 0.8194, while the previous approaches such as MD1, MD2, MD3, MD4, MD5, MD6, and MD7 obtained accuracies of 0.7866, 0.7874, 0.7879, 0.7895, 0.7946, 0.8039, and 0.8139, respectively. In the same way, for database-1, database-2, and database-3, the proposed approach performed better than other previous existing approaches shown in Table 2.

Existing methods, such as LBSP are too sensitive to changes in the area. When the proposed Equus-Jubatus optimization is compared to the performance without optimization by DNN, it shows that the performance is degraded. Additionally, methods such as MD4, MD5, MD6, and MD7 have better performance than other traditional technologies because they use an optimization algorithm called SHO, Flamingo, Herd, and Cheetah Chase. However, they obtained fewer results than with the proposed method because it uses a hybrid optimization algorithm. This improvement in the performance is due to the effective training of the classifier using the proposed Equus-Jubatus optimization. The result of proposed method is better as compare to other the state-of-the-art technique because having following advantages: 1) It is detecting minute changes and boundaries information; 2) It provide high performance with a low number of parameters; 3) Availability of skip connections require low number of training samples for segmentation; 4) It reduces complexities in the computational process using less number of parameter and faster convergence characteristics. Based on Table 2, it is clear that the presented method outperforms the state-of-the-art technique.

Table 2. Comparative analysis using database-1, database-2, database-3

Database	Methods	Accuracy	Precision	Recall	f1 Measure
Database -1 (Yambulla State Forest	LBSP (MD1)	0.831	0.768	0.785	0.835
	DNN (MD2)	0.917	0.892	0.791	0.86
	UNET (MD3)	0.921	0.894	0.808	0.86
	SHO-build on UNET (MD4)	0.922	0.895	0.842	0.86
	Flamingo-build on UNET (MD5)	0.926	0.901	0.85	0.867
	HHOA build on UNET (MD6)	0.937	0.91	0.879	0.876
	CCOA build on fusion network (MD7)	0.945	0.921	0.889	0.886
	Proposed method (MD8)	0.963	0.938	0.907	0.904
Database -2 (Natural Lake)	LBSP (MD1)	0.857	0.879	0.826	0.786
	DNN (MD2)	0.864	0.88	0.826	0.786
	UNET (MD3)	0.867	0.881	0.828	0.787
	SHO-build on UNET (MD4)	0.878	0.881	0.828	0.787
	Flamingo-build on UNET (MD5)	0.882	0.883	0.829	0.789
	HHOA build on UNET (MD6)	0.886	0.895	0.842	0.802
	CCOA build on fusion network (MD7)	0.8907	0.9006	0.847	0.807
	Proposed method (MD8)	0.895	0.906	0.852	0.812
Database -3 (Bhopal city)	LBSP (MD1)	0.786	0.757	0.881	0.836
	DNN (MD2)	0.787	0.757	0.881	0.836
	UNET (MD3)	0.787	0.758	0.882	0.837
	SHO-build on UNET (MD4)	0.789	0.758	0.882	0.837
	Flamingo-build on UNET (MD5)	0.794	0.76	0.884	0.839
	HHOA build on UNET (MD6)	0.803	0.773	0.896	0.852
	CCOA build on fusion network (MD7)	0.813	0.778	0.901	0.857
	Proposed method (MD8)	0.819	0.783	0.907	0.862

5. CONCLUSIONS

In this research, we proposed an Equus-Jubatus optimization based hybrid deep fusion model for change detection of remote sensing images. In the first part of the proposed technique, deep fusion model is used to gather the information about change in satellite images by pixel variation analysis. This fusion model is composed of FC-DenseNet, Res U-Net, U-Net, SegNet. By fusing the pre-trained models, the segmentation process is able to detect the minute changes and boundaries information. The second part of the proposed model is Equus-Jubatus optimization that integrates herding behavior of Equus or ponies and hunting behavior of Jubatus to generate the fusion parameters. Consequently, better

classification outcomes are achieved with reduced complexities in the computational process and faster convergence. The validity of the proposed strategy is demonstrated by the experimental results obtained from the remote sensing images in four distinct databases. In comparison with previous techniques such as MD1, MD2, MD3, MD4, MD5, MD6, and MD7, our proposed approach (MD8) shows outstanding results with enhanced accuracy, precision, recall, and f1-measure performance.

In the future, a highly-advanced image feature extraction technique will be utilized, further promoting the classification performance.

REFERENCES

[1] Lv, Z.Y., Shi, W., Zhang, X., Benediktsson, J.A. (2018). Landslide inventory mapping from bitemporal high-resolution remote sensing images using change detection and multiscale segmentation. IEEE Journal of Selected Topics in Applied Earth Observations and Remote Sensing, 11(5): 1520-1532. https://doi.org/10.1109/JSTARS.2018.2803784

[2] Chen, J., Yuan, Z., Peng, J., Chen, L., Huang, H., Zhu, J., Liu, Y., Li, H. (2020). DASNet: Dual attentive fully convolutional Siamese networks for change detection in high-resolution satellite images. IEEE Journal of Selected Topics in Applied Earth Observations and Remote Sensing, 14: 1194-1206. https://doi.org/10.1109/JSTARS.2020.3037893

[3] Venkatachalam, J., Chandrabose, S. (2023). Optimizing region detection in enhanced infrared images using deep learning. Revue d'Intelligence Artificielle, 37(4): 1015-1021. https://doi.org/10.18280/ria.370423

[4] Khelifi, L., Mignotte, M. (2020). Deep learning for change detection in remote sensing images: Comprehensive review and meta-analysis. IEEE Access, 8: 126385-126400. https://doi.org/10.1109/ACCESS.2020.3008036

[5] Alcantarilla, P.F., Stent, S., Ros, G., Arroyo, R., Gherardi, R. (2018). Street-view change detection with deconvolutional networks. Autonomous Robots, 42: 1301-1322. https://doi.org/10.1007/s10514-018-9734-5

[6] Said, N., Ahmad, K., Riegler, M., Pogorelov, K., Hassan, L., Ahmad, N., Conci, N. (2019). Natural disasters detection in social media and satellite imagery: A survey. Multimedia Tools and Applications, 78: 31267-31302. https://doi.org/10.1007/s11042-019-07942-1

[7] Ye, S., Rogan, J., Zhu, Z., Eastman, J.R. (2021). A near-real-time approach for monitoring forest disturbance using Landsat time series: Stochastic continuous change detection. Remote Sensing of Environment, 252: 112167. https://doi.org/10.1016/j.rse.2020.112167

[8] Wang, D., Chen, X., Jiang, M., Du, S., Xu, B., Wang, J. (2021). ADS-Net: An Attention-Based deeply supervised network for remote sensing image change detection. International Journal of Applied Earth Observation and Geoinformation, 101: 102348. https://doi.org/10.1016/j.jag.2021.102348

[9] Qin, D., Zhou, X., Zhou, W., Huang, G., Ren, Y., Horan, B., He, J., Kito, N. (2018). MSIM: A change detection framework for damage assessment in natural disasters. Expert Systems with Applications, 97: 372-383. https://doi.org/10.1016/j.eswa.2017.12.038

[10] Ramdass, P., Ganesan, G. (2023). Leveraging neighbourhood component analysis for optimizing multilayer feed-forward neural networks in heart disease prediction. Mathematical Modelling of Engineering Problems, 10(4): 1317-1323. https://doi.org/10.18280/mmep.100425

[11] Su, M.C., Huang, D.Y., Chen, J.H., Lu, W.Z., Tsai, L.C., Lin, J.Z. (2011). Mapping multi-spectral remote sensing images using rule extraction approach. Expert Systems with Applications, 38(10): 12917-12922. https://doi.org/10.1016/j.eswa.2011.04.086

[12] Zheng, Z., Wan, Y., Zhang, Y., Xiang, S., Peng, D., Zhang, B. (2021). CLNet: Cross-layer convolutional neural network for change detection in optical remote sensing imagery. ISPRS Journal of Photogrammetry and Remote Sensing, 175: 247-267. https://doi.org/10.1016/j.isprsjprs.2021.03.005

[13] Chen, H., Qi, Z., Shi, Z. (2021). Remote sensing image change detection with transformers. IEEE Transactions on Geoscience and Remote Sensing, 60: 1-14. https://doi.org/10.1109/TGRS.2021.3095166

[14] Lei, T., Zhang, Q., Xue, D., Chen, T., Meng, H., Nandi, A.K. (2019). End-to-end change detection using a symmetric fully convolutional network for landslide mapping. In ICASSP 2019-2019 IEEE International Conference on Acoustics, Speech and Signal Processing (ICASSP), Brighton, UK, pp. 3027-3031. https://doi.org/10.1109/ICASSP.2019.8682802

[15] Lei, T., Zhang, Y., Lv, Z., Li, S., Liu, S., Nandi, A.K. (2019). Landslide inventory mapping from bitemporal images using deep convolutional neural networks. IEEE Geoscience and Remote Sensing Letters, 16(6): 982-986. https://doi.org/10.1109/LGRS.2018.2889307

[16] Ren, C., Wang, X., Gao, J., Zhou, X., Chen, H. (2020). Unsupervised change detection in satellite images with generative adversarial network. IEEE Transactions on Geoscience and Remote Sensing, 59(12): 10047-10061. https://doi.org/10.1109/TGRS.2020.3043766

[17] Sheoran, S., Mittal, N., Gelbukh, A. (2021). Improved change detection in remote sensed images by artificial intelligence techniques. Journal of the Indian Society of Remote Sensing, 49(9): 2079-2092. https://doi.org/10.1007/s12524-021-01374-x

[18] Brahimi, S., Ben Aoun, N., Benoit, A., Lambert, P., Ben Amar, C. (2019). Semantic segmentation using reinforced fully convolutional densenet with multiscale kernel. Multimedia Tools and Applications, 78: 22077-22098. https://doi.org/10.1007/s11042-019-7430-x

[19] Badrinarayanan, V., Kendall, A., Cipolla, R. (2017). Segnet: A deep convolutional encoder-decoder architecture for image segmentation. IEEE Transactions on Pattern Analysis and Machine Intelligence, 39(12): 2481-2495. https://doi.org/10.1109/TPAMI.2016.2644615

[20] Zhou, J., Lu, Y., Tao, S., Cheng, X., Huang, C. (2021). E-Res U-Net: An improved U-Net model for segmentation of muscle images. Expert Systems with Applications, 185: 115625. https://doi.org/10.1016/j.eswa.2021.115625

[21] Vasantrao, C.P., Gupta, N. (2023). Wader hunt optimization based UNET model for change detection in satellite images. International Journal of Information Technology, 15(3): 1611-1623. https://doi.org/10.1007/s41870-023-01167-0

[22] Sacharisa, S., Kartowisastro, I.H. (2023). Enhanced spine segmentation in scoliosis X-ray images via U-Net. Ingénierie des Systèmes d'Information, 28(4): 1073-1079. https://doi.org/10.18280/isi.280427

[23] MiarNaeimi, F., Azizyan, G., Rashki, M. (2021). Horse herd optimization algorithm: A nature-inspired algorithm for high-dimensional optimization problems. Knowledge-Based Systems, 213: 106711. https://doi.org/10.1016/j.knosys.2020.106711

[24] Goudhaman, M. (2018). Cheetah chase algorithm (CCA): a nature-inspired metaheuristic algorithm. International Journal of Engineering & Technology, 7(3): 1804-1811. https://doi.org/10.14419/ijet.v7i3.18.14616

[25] Kundu, K., Halder, P., Mandal, J.K. (2021). Change detection and patch analysis of sundarban forest during 1975–2018 using remote sensing and GIS data. SN Computer Science, 2: 1-14. https://doi.org/10.1007/s42979-021-00749-8

[26] Gupta, N., Pillai, G.V., Ari, S. (2018). Change detection in optical satellite images based on local binary similarity pattern technique. IEEE Geoscience and Remote Sensing Letters, 15(3): 389-393. https://doi.org/10.1109/LGRS.2018.2789404

[27] Shaik, K.S., Thumboor, N.S.K., Veluru, S.P., Bommagani, N.J., Sudarsa, D., Muppagowni, G.K. (2023). Enhanced SVM model with Orthogonal Learning Chaotic Grey Wolf Optimization for cybersecurity intrusion detection in Agriculture 4.0. International Journal of Safety and Security Engineering, 13(3): 509-517. https://doi.org/10.18280/ijsse.130313

[28] Zulfiqar, A., Ghaffar, M.M., Shahzad, M., Weis, C., Malik, M.I., Shafait, F., Wehn, N. (2021). AI-ForestWatch: Semantic segmentation based end-to-end framework for forest estimation and change detection using multi-spectral remote sensing imagery. Journal of Applied Remote Sensing, 15(2): 024518-024518. https://doi.org/10.1117/1.JRS.15.024518

[29] Kumar, S., Arya, S., Jain, K. (2022). A SWIR-based vegetation index for change detection in land cover using multi-temporal Landsat satellite dataset. International Journal of Information Technology, 14: 2035-2048. https://doi.org/10.1007/s41870-021-00797-6

[30] Reyes, D., Bone, C., Padilla-Almeida, O., Ananganó, P., Guamán, S., Kirby, E., Toulkeridis, T. (2019). Use of multitemporal indexes in the identification of forest fires-a case study of Southern Chile. In 2019 Sixth International Conference on eDemocracy & eGovernment (ICEDEG), Quito, Ecuador, pp. 203-210. https://doi.org/10.1109/ICEDEG.2019.8734443

[31] Xie, Q., Dash, J., Huang, W., Peng, D., Qin, Q., Mortimer, H., Casa, R., Pignatti, S., Laneve, G., Pascucci, S., Dong, Y., Ye, H. (2018). Vegetation indices combining the red and red-edge spectral information for leaf area index retrieval. IEEE Journal of Selected Topics in Applied Earth Observations and Remote Sensing, 11(5): 1482-1493. https://doi.org/10.1109/JSTARS.2018.2813281

[32] Rosso, P., Nendel, C., Gilardi, N., Udroiu, C., Chlebowski, F. (2022). Processing of remote sensing information to retrieve leaf area index in barley: A comparison of methods. Precision Agriculture, 23(4): 1449-1472. https://doi.org/10.1007/s11119-022-09893-4

[33] Vasantrao, C.P., Gupta, N., Jonnala, N.S., Mishra, A.K. (2023). Dual adaptive model for change detection in multispectral images. In 2023 Second International Conference on Electrical, Electronics, Information and Communication Technologies (ICEEICT), Trichirappalli, India, pp. 1-6. https://doi.org/10.1109/ICEEICT56924.2023.10156920

[34] Zeyad, A.M.A., Biradar, A. (2023). A hybrid text summarization approach using neural networks and metaheuristic algorithms. International Journal of Safety and Security Engineering, 13(3): 479-489. https://doi.org/10.18280/ijsse.130310

[35] Gupta, N., Ari, S., Panigrahi, N. (2019). Change detection in landsat images using unsupervised learning and RBF-based clustering. IEEE Transactions on Emerging Topics in Computational Intelligence, 5(2): 284-297. https://doi.org/10.1109/TETCI.2019.2932087

[36] https://gisgeography.com/usgs-earth-explorer-download-free-landsat-imagery/.

[37] Gupta, N., Pillai, G.V., Ari, S. (2018). Change detection in Landsat images based on local neighbourhood information. IET Image Processing, 12(11): 2051-2058. https://doi.org/10.1049/iet-ipr.2018.5524

[38] Li, X., Du, Z., Huang, Y., Tan, Z. (2021). A deep translation (GAN) based change detection network for optical and SAR remote sensing images. ISPRS Journal of Photogrammetry and Remote Sensing, 179: 14-34. https://doi.org/10.1016/j.isprsjprs.2021.07.007

[39] Wang, J., Wang, Y., Chen, B., Liu, H. (2021). LCS-EnsemNet: A semisupervised deep neural network for SAR image change detection with dual feature extraction and label-consistent self-ensemble. IEEE Journal of Selected Topics in Applied Earth Observations and Remote Sensing, 14: 11903-11925. https://doi.org/10.1109/JSTARS.2021.3122461

[40] Ren, J., Tong, L., Li, Y., Yuan, L., Si, Y. (2021). Improved unet combining dropout and acnet for remote sensing image change detection. In 2021 IEEE International Geoscience and Remote Sensing Symposium IGARSS, Brussels, Belgium, pp. 4380-4383. https://doi.org/10.1109/IGARSS47720.2021.9553666

[41] Dhiman, G., Kumar, V. (2017). Spotted hyena optimizer: A novel bio-inspired based metaheuristic technique for engineering applications. Advances in Engineering Software, 114: 48-70. https://doi.org/10.1016/j.advengsoft.2017.05.014

[42] Zhiheng, W., Jianhua, L. (2021). Flamingo search algorithm: A new swarm intelligence optimization algorithm. IEEE Access, 9: 88564-88582. https://doi.org/10.1109/ACCESS.2021.3090512